An Overview of Micro Tribology Mechanical Theory with and without Adhesion

Ryan P. Hennessy

Project Report
ME-5656: Contact Mechanics
November 29, 2011

1.   Introduction

The contact occurring in an RF MEMS microswitch presents an intricate tribological environment. When such a switch is closed, the contact bump of the switch is held firmly against the drain such that electrical current can flow. If the surfaces are rough, the real contact area is comprised of the sum of many individual asperity contact areas. Joule heating due to the flow of current causes a temperature distribution near the contact above that of the ambient. This resulting thermal-elastic expansion can change the contact area which, in turn, affects the contact resistance and Joule heating. Thermal softening can cause reshaping of the contact region thereby affecting adhesion and contact failure. Thus, the contact of the microswitch, such as that presented in Figure 1, is significantly affected by the thermal, electrical, and mechanical domains.

This report will summarize the theory that governs mechanical contact between two surfaces. The electrical and thermal domains, though relevant, will not be presented as they are out of the scope of this course (**SEE APPENDIX**). However, both single and mutli-asperity models will be covered, both with and without adhesion. This body of knowledge will form a broad and full understanding of micro-tribology in the purely mechanical domain. It should be noted that this report will be a starting point for my literature review, and thus the focus of this review will be on presenting the pertinent equations.
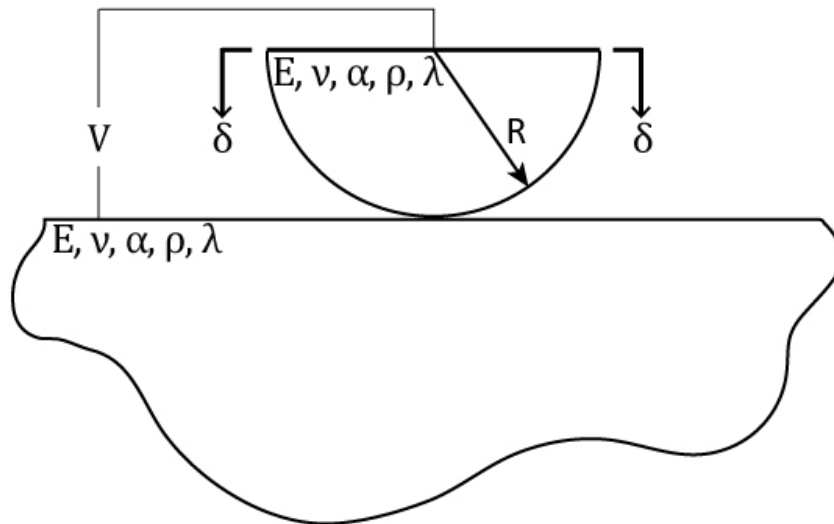
Figure 1: A thermal-electrical-mechanical coupled-field Contact

2.   Single Asperity Models

In this section, single asperity models predicting the mechanical behavior of two objects in contact will be presented. It is important to note that all of these models assume steady state, linear, elastic, isotropic material behavior.

(2.1) *Hertz Contact*

In 1882, on his Christmas break from graduate school, Heinrich Hertz developed a model to understand the effects on optical properties of holding force on stacked lenses [1].
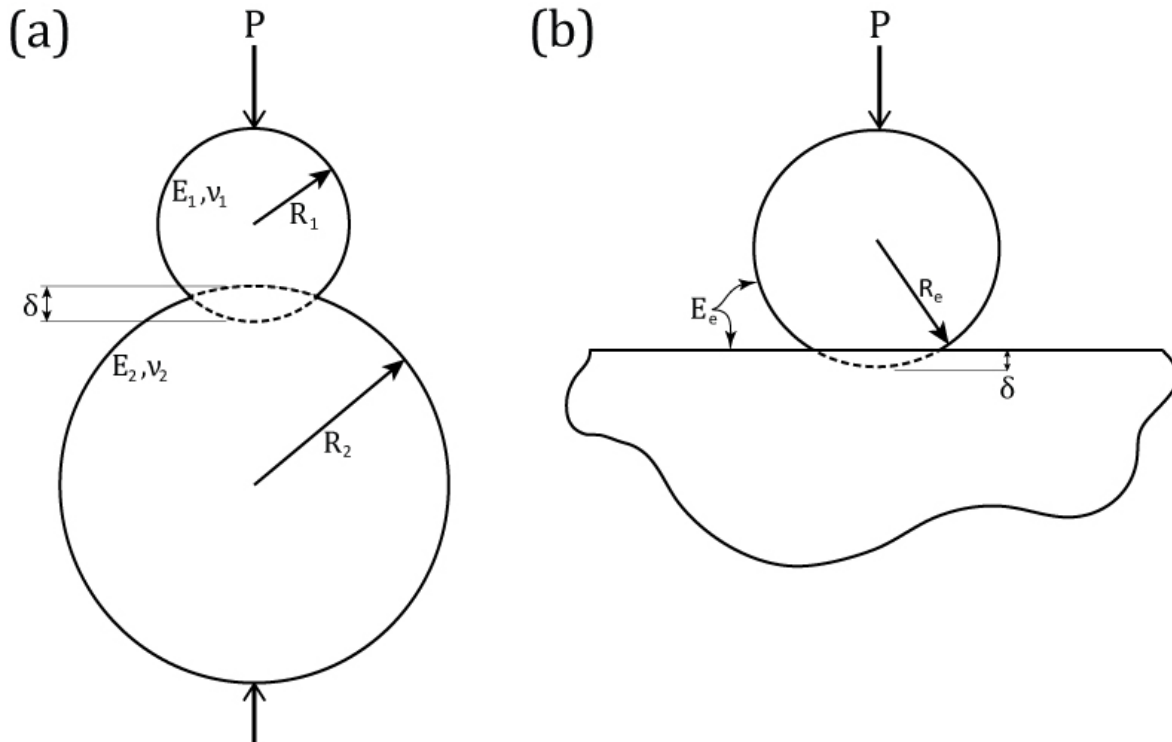
Figure 2: (a) Two spheres being pressed against each other (b) A sphere being pressed into a half-space

Consider a system composed of two spheres being pressed against each other with a force, P, or a prescribed interference, δ, as depicted in Figure 2a. The contact spot between the two spheres will be a circle of radius a. The normal traction force profile (IE, the normal stress profile on the surfaces of the sphere) inside the circular contact area is assumed to be parabolic

$$p(r) = p_0 \left(1 - \left(\frac{r}{a}\right)^2\right)^{1/2} \tag{1}$$

$$p_0 = \left(\frac{3P}{2\pi a^2}\right) \tag{2}$$

as depicted in Figure 3.

Contact Spot

Using this formulation, the contact radius, a, for a prescribed interference, δ,

$$a = (R_e \delta)^{1/2} \tag{3}$$

Alternately, if a downward contact force, P, is applied to the hemisphere

$$a = \left(\frac{3PR_e}{4E_e}\right)^{1/3} = \left(\frac{PR_e}{K}\right)^{1/3} \tag{4}$$

where the effective radius (R_e), and effective modulus (E_e) are defined respectively as

$$R_e = \left(\frac{1}{R_1} + \frac{1}{R_2}\right)^{-1} \tag{5}$$

$$E_e = \left(\frac{1-v_1^2}{E_1} + \frac{1-v_2^2}{E_2}\right)^{-1} \tag{6}$$

$$K = \frac{4}{3}E_e \tag{7}$$

In Equation (4) above, E is the modulus of elasticity and v is Poisson's ratio. The numerical subscripts correspond to the component of the contact. Note that the effective radius and effective modulus make the schematics of Figure 3a and 3b exactly equivalent.

Additionally, the amount of holding force necessary to generate a prescribed interference is defined as

$$P = \left(\frac{4E_e R_e^{1/2}}{3}\right) \delta^{3/2} \tag{8}$$

In this form, if the interference is viewed as a displacement, the contact can be viewed as a non-linear spring with a non-linear spring constant being ($4E_e^2 R_e^2/3$).

Note that this model is purely elastic and does not include surface forces such as adhesion. At the micro and nano scales, adhesion forces become extremely important because of scaling effects. Essentially there are two types of adhesion to consider: dry adhesion, which results from van der Waals forces (attraction and repulsion forces due to molecular interactions), and wet adhesion, which result

from meniscus forces. The next four models present ways of calculating the effect of dry adhesion acting on a contact. As it will be explained, the characteristics of the contact determine which model to apply.

(2.2) *Bradley Model*

The Bradley model attempts to find the tensile force between two perfectly-smooth rigid spheres from the Leonard-Jones potential [2]. Using the Leonard-Jones potential, the force between two atomic planes, F, separated by distance z is expressed as

$$F = \frac{8\Delta\gamma}{3z_0}\left(\left(\frac{z}{z_0}\right)^{-9} - \left(\frac{z}{z_0}\right)^{-3}\right)$$

(9)

Where z_0 is the equilibrium spacing of atomic planes and

$$\Delta\gamma = \gamma_1 + \gamma_2 - \gamma_{12}$$

(10)

is the work of adhesion, and γ is the surface energy. A non-dimensional plot of this relationship is presented in Figure 4.
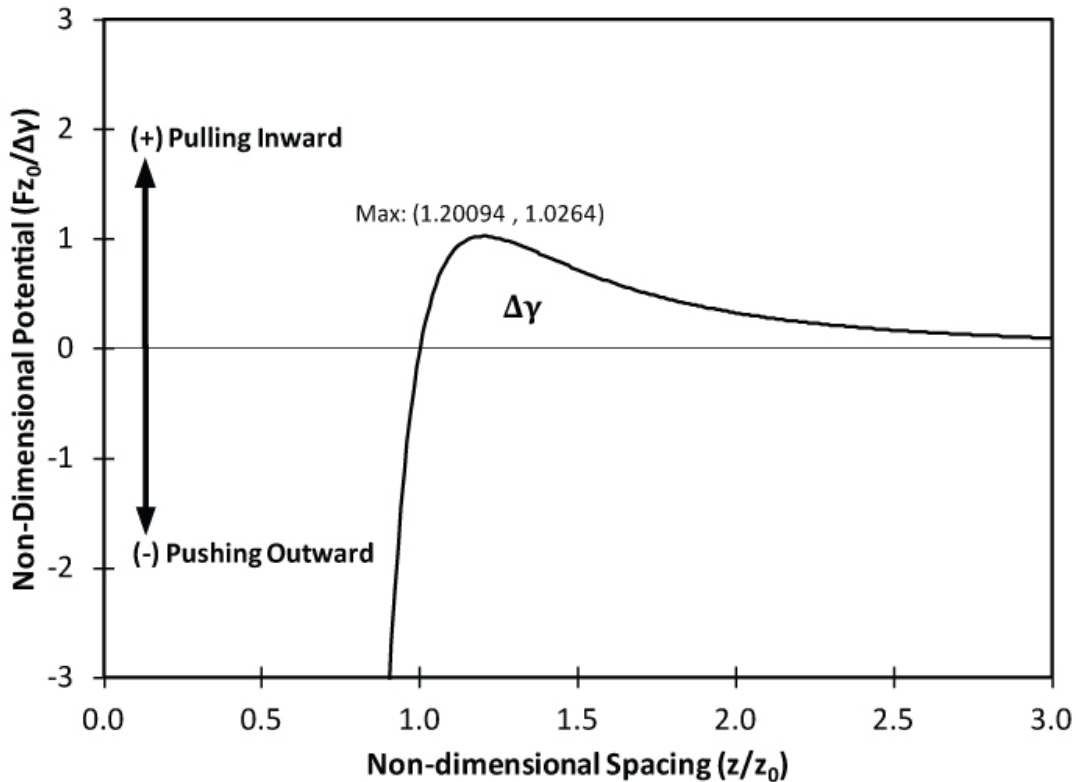
Figure 4: Non-dimensional plot of the Leonard-Jones potential

For two identical materials, $\Delta\gamma = 2\gamma$. Using this formulation, the adhesion force between two spheres can be calculated as

$$F_{Bradley} = \frac{8\Delta\gamma\pi R_e}{3}\left(\left(\frac{1}{4}\right)\left(\frac{z}{z_0}\right)^{-8} - \left(\frac{z}{z_0}\right)^{-2}\right) \tag{11}$$

The two spheres separate when $z = z_0$, leading to the calculation of a pull-off force

$$F_{\text{Pull-Off, Bradley}} = 2\pi\Delta\gamma R_e \tag{12}$$

For application purposes, this model is only useful in situations where deformation is negligible. The next few models include deformation.

(2.3) *Johnson-Kendall-Roberts (JKR)*

The JKR model includes elastic deformation and treats the effect of adhesion as surface energy only [3]. In this model, adhesive force (attractive tensile forces) are only considered in the contact region, and not considered at all in the separation region. Using this formulation, the total energy equilibrium equation can be solved. Figure 5 represents a schematic of the resulting contact spot.
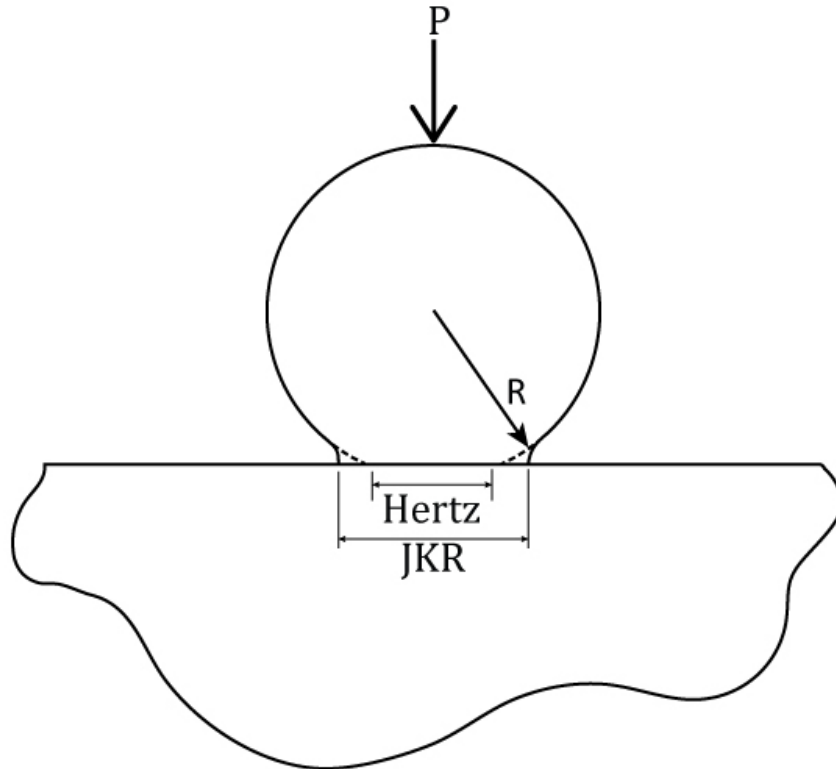
Figure 5: Hertz contact spot vs JKR contact spot with 'necking' due to adhesive forces

For a prescribed contact force

$$a = \left(\frac{R_e}{K}\left(P + 3\pi\Delta\gamma R_e + (6\pi\Delta\gamma R_e P + (3\pi\Delta\gamma R_e)^2)^{1/2}\right)\right)^{1/3} \tag{13}$$

Alternately, for a prescribed interference

$$a = \left(\delta R_e + \left(\frac{8\pi a \Delta\gamma R_e^2}{3K} \right)^{1/2} \right)^{1/2} \tag{14}$$

$$\delta = \frac{a^2}{R_e} - \left(\frac{8\pi a \Delta\gamma}{3K} \right)^{1/2} \tag{15}$$

Comparing these Equations 2 and 1, respectively, the additional adhesion terms become apparent. Additionally, the pull-off force is

$$F_{\text{Pull-Off, JKR}} = 1.5\pi\Delta\gamma R_e \tag{16}$$

It is important to note that while all of the other adhesion models discussed in this review allow for the existence of a pull-in force, the JKR model does not

(2.4) *Derjaguin-Muller-Toporov (DMT)*

The DMT model assumes that adhesive tensile stresses exist outside of the contact region (IE, tensile forces in the separation region), while the stresses inside the contact region remain identical to Hertz (IE, parabolic normal force distribution) [4], as shown in Figure 6.
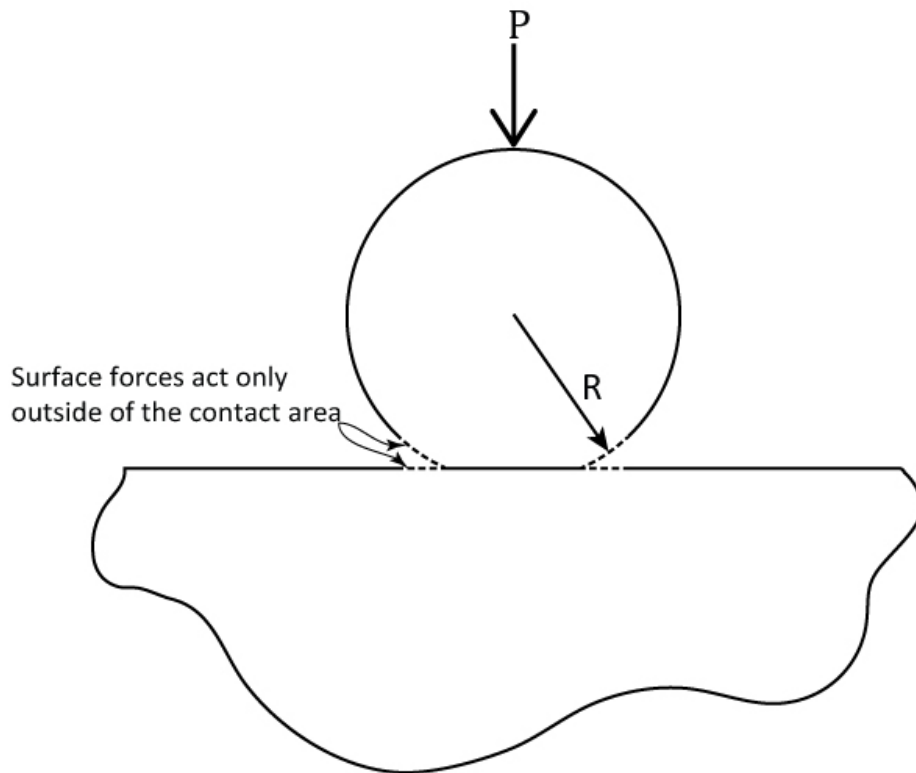
Figure 6: DMT contact where the dashed lines indicate the regions in which adhesive forces act

Assuming this stress profile, the contact area for a prescribe contact force is

$$a = \left(\frac{R_e}{K} (P + 2\pi \Delta \gamma R_e) \right)^{1/3} \tag{17}$$

$$\delta = \frac{Ka^3}{R_e} - 2\pi \Delta \gamma R_e \tag{18}$$

while the contact area for a prescribed interference is

$$a = (R_e \delta)^{1/2} \tag{19}$$

Note that Equation 19 is identical to Equation 1; again, this is because the stress profile inside the contact is assumed to be identical to that of Hertz contact. Additionally, the pull-off force is

$$F_{\text{Pull-Off, DMT}} = 2\pi \Delta \gamma R_e \tag{20}$$

(2.5) *Tabor Parameter*

The DMT and JKR adhesions theories were the cause of a lot of heated debate because they are seemingly in direct contrast with each other [5]. This was not until it was discovered that these theories are actually the limit cases of opposing ends of the same behavior spectrum. To distinguish the appropriate applications for the JKR and DMT theories, the Tabor parameter, μ, was created

$$\mu = \left(\frac{\Delta \gamma^2 R_e}{E_e^2 z_0^3} \right)^{1/3} \tag{21}$$

The Tabor parameter is the physical equivalent to the ratio of normal elastic deformation caused by adhesion to the spatial range of the adhesion forces [6].

Tabor parameter theory states that for μ values much less than one (stiff solids, small effective radius of curvature, weak energy of adhesion), the DMT model is appropriate. Alternately, for μ values much greater than one (compliant solids, large effective radius of curvature, large energy of adhesion), the JKR model is appropriate.

(2.6) *Maugis-Dugdale Model (MD)*

For intermediate values of the Tabor parameter, μ, Maugis [7] approximated the behavior of surface interaction using a Dugdale cohesive zone approximation. In this model, Maugis defines an elasticity parameter

$$\lambda = 2\sigma_0 \left(\frac{R_e}{\Delta \gamma K^2} \right)^{1/3} \tag{22}$$

where σ_0 is a constant adhesion stress that acts over a range of δ_t, resulting in the work of adhesion $\Delta \gamma = \sigma_0 \delta_t$. By choosing σ_0 to equal the minimum adhesion stress for a Lennard-Jones potential (with

equilibrium spacing of z_0), it follows that δ_t =0.97z_0, making λ=1.1570μ. This leads to a the following system of three equations

$$1 = \frac{\lambda a^2}{2}\left(\frac{K}{\pi R_e^2 \Delta \gamma}\right)^{3/2}\left(\sqrt{m^2-1}+(m^2-2)\operatorname{atan}\sqrt{m^2-1}\right)$$
$$+\frac{4\lambda a^2}{3}\left(\frac{K}{\pi R_e^2 \Delta \gamma}\right)^{1/3}\left(1-m+\sqrt{m^2-1}\operatorname{atan}\sqrt{m^2-1}\right) \tag{23}$$

$$P = \frac{Ka^3}{R} - \lambda a^2 \left(\frac{\pi\Delta\gamma K^2}{2}\right)^{3/2}\left(\sqrt{m^2-1}+m^2\operatorname{atan}\sqrt{m^2-1}\right) \tag{24}$$

$$\delta = \frac{a^2}{R} - \frac{4\lambda a}{3}\left(\frac{\pi\Delta\gamma}{RK}\right)^{1/3}\sqrt{m^2-1} \tag{25}$$

where m = a/c, or the ratio of the contact radius to the cohesive zone radius. In this system of equations, if the elasticity parameter, λ, is not known before solving the problem, it must be found by iteratively. This makes finding a solution to a given problem cumbersome. However, it is generally agreed that this model is generally the best because this model encompasses the entire range of adhesion behavior. More specifically, for $\lambda > 5$, the JKR model applies, and for $\lambda < 0.1$, the DMT model applies. Figure 7 is a convenient adhesion map depicting the appropriate property sets in which to use the different adhesion models.
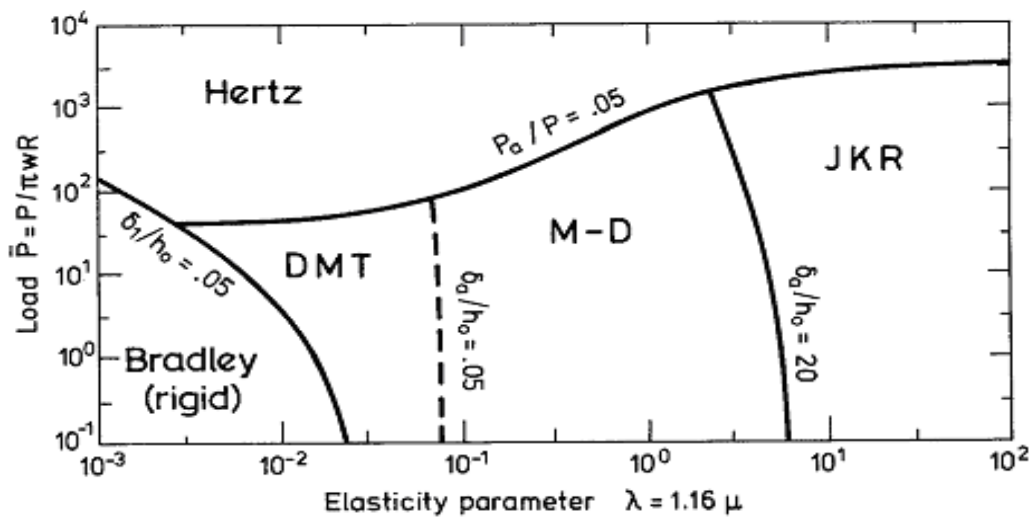
Figure 7: An Adhesion map as presented in [8]

Additionally, Figure 8 provides a representative plot of force versus displacement for the different adhesion models.
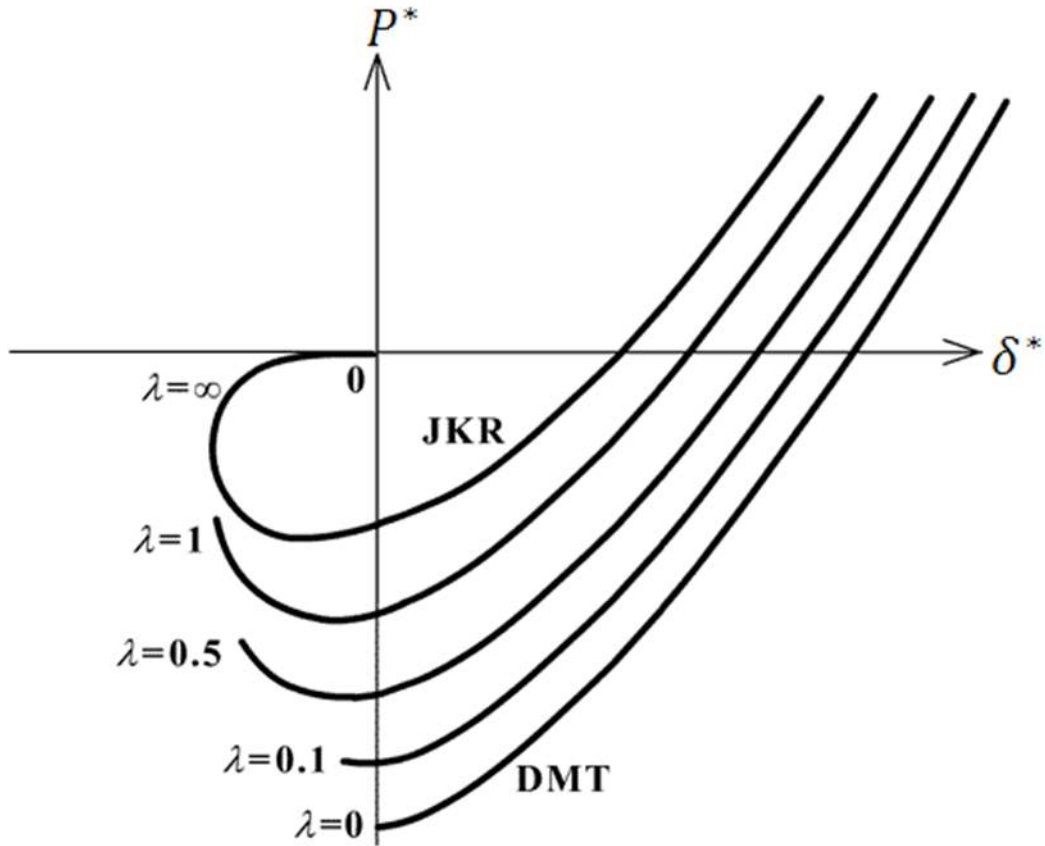
Figure 8: Normalized force versus normalized interference for JKR, DMT, and MD adhesion models

where the normalized values are defined as

$$P^* = \frac{P}{\pi R_e \Delta \gamma} \tag{26}$$

$$\delta^* = \frac{\delta}{\left(\frac{\pi^2 R_e \Delta \gamma^2}{K^2}\right)^{1/3}} \tag{27}$$

(2.7) *Carpick-Ogletree-Salmeron (COS)*

Because of the cumbersome nature of solving the Maugis system, Carpick, Ogletree, and Salmeron (COS) [9] used numerical software and curve fitting to develop a general approximation equation to determine the contact area. They showed that the Maugis formulation could be approximated using the generalized transition equation

$$a = a_{0(\alpha)} \left(\frac{\alpha + \left(1 - P/P_{c(\alpha)}\right)^{1/2}}{1 + \alpha} \right)^{2/3} \tag{28}$$

where α is another transition parameter and a_0 is the contact area at zero load. The α = 0 case corresponds exactly to the DMT formulation, while the α = 1 case corresponds exactly to the JKR formulation. The relationship between Maugis' elasticity parameter, and the COS transition parameter is given by

$$\lambda = -0.924 \ln(1 - 1.02\alpha) \tag{29}$$

Using this model, computation time is greatly reduced which accuracy is retained. The step-by-step application process is outlined in the paper.

3. Multi Asperity Models

In this section, multi-asperity models predicting the mechanical behavior of two objects in contact will be presented. Again, only steady state, linear, elastic, isotropic material behavior is considered in these models.

(3.1) Greenwood and Williamson

The Greenwood and Williamson [10] model attempts to describe the behavior when two rough surfaces come into contact, as depicted in Figure 9a. This model makes the following assumptions:

- Contact is between a plane and a nominally flat surface with a large number (N) asperities
- All of the asperities are locally spherical
- All asperity summits have the same radius (R_e)
- The asperity height varies randomly, thus the probability of making contact at any given asperity of height z is

$$\mathrm{prob}(z > d) = \int_d^\infty \phi(z) dz \tag{30}$$

where $\phi(z)$ is the probability that a particular asperity has a height between z and dz above some reference plane and d is the separation between the reference planes of the two contacting surfaces, as depicted in Figure 9b. This means that the expected number of contacts n is

$$n = N \int_d^\infty \phi(z) dz \tag{31}$$

- All asperity contacts are considered Hertz contacts
- All asperities are sufficiently separated to be mechanically independent

Next, a normalized separation is defined as

$$h = {}^d\!/_\sigma \tag{32}$$

where σ is the standard deviation of the peak height probability density function $\phi(z)$. If the 'apparent' or nominal contact area is A_a, the asperity density can be defined as

$$\eta = {}^{N}\!/\!_{A_a} \tag{33}$$

(a)
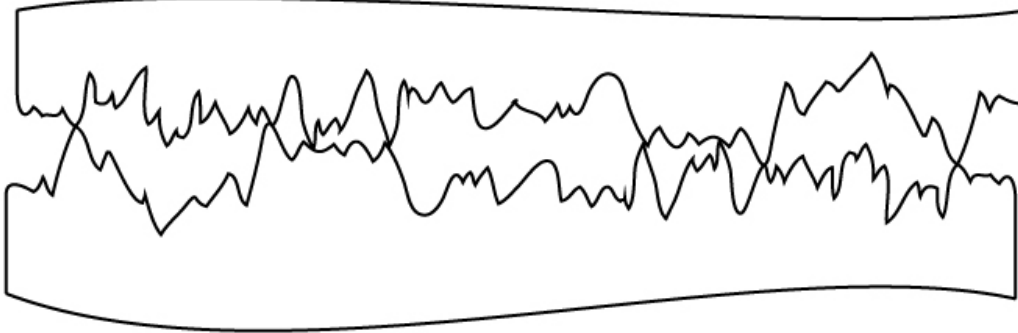
(b)
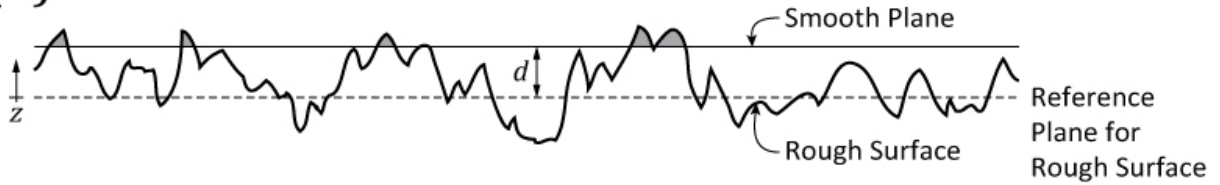
Figure 9: (a) Two rough surfaces in contact (b) Contact of an equivalent rough surface with a smooth plane, only the tallest asperities make contact and thus support the entire load – those asperity peaks are shaded in gray

With these definitions and the aforementioned assumptions, the following relations for total load, P, number of contacts, n, real (or 'True') contact area, A_r, can be written as

$$n = \eta A_a F_0(h) \tag{34}$$

$$A_r = \pi \eta A_a R_e \sigma F_1(h) \tag{35}$$

$$P = \frac{4}{3}\eta A_a E_e R_e^{1/2} \sigma^{3/2} F_{3/2}(h) \tag{36}$$

where

$$F_n(h) = N \int_h^{\infty} (z^* - h)^n \phi^*(z^*)dz^* \tag{37}$$

In this equation $\phi^*(z^*)$ represents the normalized asperity height distribution. And

$$z^* = \frac{z - m}{\sigma} \tag{38}$$

Again, z is a variable asperity height with respect to a reference plane, m is the mean of the height distribution, and σ is the standard deviation of the height distribution.

When the asperity heights follow an exponential distribution (which is a loose approximation of the uppermost 25% of asperity heights in a Gaussian distribution)

$$\phi^*(z^*) = e^{-z^*} \tag{39}$$

the equations for total load, P, number of contacts, n, real contact area, A_r, reduce to

$$n = \eta A_a e^{-h} \tag{40}$$

$$A_r = \pi \eta R_e \sigma A_a e^{-h} \tag{41}$$

$$P = \pi^{1/2} \eta R_e \sigma A_a E_e \left(\sigma/R_e\right)^{1/2} e^{-h} \tag{42}$$

This result is so significant because it shows a direct linear relationship between contact force and real contact area as well as contact force and the number of contact spots. Thus the average size of the contact spots and the contact pressure are independent of the load. It is extremely important to note that this result does not depend on the particular surface model or deformation mode. Rather, this result holds for an exponential distribution of asperity heights as long as all of the asperity contacts obey the same area / compliance and load / compliance laws! Moreover, these results suggest that the laws of Coulomb friction are indeed accurate.

This paper goes on to discuss the results from a Gaussian distribution of asperity heights. It turns out that these results come out close to those results for an exponential distribution.

(3.2) Multi-Asperity Models with Adhesion

Since the pioneering work of Greenwood and Williamson, authors have used the same statistical approach to incorporating adhesion into multi-asperity system. For example, Fuller *et al* in [11] explores a multi-asperity model with JKR adhesive contact instead of Hertz contacts. In 1996, Maugis in [12] presented a multi-asperity model of the Greenwood and Williamson approach with DMT adhesive contacts instead of Hertz contacts. And finally, Morrow *et al* in [13] created a multi-asperity model using Maugid-Dugdale adhesive contact.

4. Conclusion

In conclusion, this paper reviewed the fundamental theories that govern the mechanics of contact with and without adhesion. In the context of microswitch contacts, a single asperity model could be taken as either a smooth contact bump contacting a flat surface, or a single asperity of a rough contact bump contacting a flat surface. It was shown how these single asperity models were applied into multi-asperity models via some simple assumptions and statistical math. By applying models, a better understanding of the mechanics of a microswitch contact can be achieved.

REFERENCES

[1] H. Hertz, Über die berührung fester elastischer Körper (On the contact of rigid elastic solids). In: *Miscellaneous Papers*. Jones and Schott, Editors, *J. reine und angewandte Mathematik* 92, Macmillan, London (1896), p. 156 English translation: Hertz, H. (1882)

[2] Bradley, R.S., 1932, Philosophical Magazine, **13**, pp. 853-862

[3] Johnson, K.L., Kendall, K., and Roberts, A.D., 1971, "Surface Energy and the Contact of Elastic Solids," Proceedings of the Royal Society of London, A324, pp. 301-313.

[4] Derjaguin, B.V., Muller, V.M., Toporov, Y.P., 1975, J. Coll. Interf. Sci., 53, pp. 314-326.

[5] Tabor, D., 1977, *Surface forces and surface interactions*, Journal of Colloid and Interface Science, 58(1), pp. 2-13.

[6] Grierson, Flater, & Carpick – J. Adhesion Sci Technology, 2005

[7] Maugis, D., 1996, "On the Contact and Adhesion of Rough Surfaces," Journal of Adhesion Science and Technology, 10, pp. 161-175

[8] K.L. Johnson and J.A. Greenwood, J. of Colloid Interface Sci., 192, pp. 326-333, 1997

Muller, V.M., Derjaguin, B.V., Toporov, Y.P., 1983, Coll. and Surf., 7, pp. 251-259.

[9] R. W. Carpick, D. F. Ogletree, M. Salmeron, J. Colloid Interf. Sci. 211, 395 (1999).

[10] Greenwood and Williamson, 1966, *Proceedings of the Royal Society of London,* A295, pp. 300-319

[11] Fuller, K.N.G., and Tabor, D., 1975, *Proc. Royal Society of London,* **A345**, pp. 327-342.

[12] Maugis, D., 1996, "On the Contact and Adhesion of Rough Surfaces," Journal of Adhesion Science and Technology, 10, pp. 161-175

[13] Morrow, C., Lovell, M., and Ning, X., 2003, J. of Physics D: Applied Physics, 36, pp. 534-540.

5. Electrical Domain

(5.1) *Constriction Resistance (Maxwell Spreading Resistance)*

In the electrical domain, the contact resistance governs the amount of electric current that flows through the contact area. This contact resistance is comprised of two components: effects due to imperfect electrical contact (such as resistive contaminant films), and effects due to the converging and diverging of current paths through the constriction. Assuming perfect electrical contact, the contact area can be modeled as a current constriction. If the contact radius is known and is much larger than the electron mean-free-path of the contact material, the contact resistance can be calculated by the Maxwell spreading resistance

$$\Omega_{Maxwell} = \frac{\rho_1 + \rho_2}{4a} \tag{43}$$

for the constriction resistance between two identical half-spaces. Where ρ_1 and ρ_2 are the electrical resistivities corresponding to the contact components.
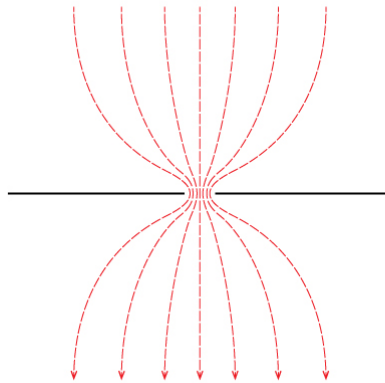
Figure 10: Electrical current line through a constriction

If the contact material is the same for both components of the contact, the Maxwell spreading resistance simplifies to

$$\Omega_{Maxwell} = \frac{\rho}{2a} \tag{44}$$

(5.2) *Constriction Resistance (Sharvin Regime)*

If the contact radius is small compared to the electron mean-free-path of the contact material, λ, current is conducted via electrons projected ballistically through the contact without scattering. The effective mean free path of the contact can be calculated as

$$\lambda_e = \frac{\lambda_1 + \lambda_2}{2} \tag{45}$$

In this case, the contact resistance is calculated using the Sharvin model.

$$\Omega_{Sharvin} = \frac{\lambda_e(\rho_1 + \rho_2)}{2a} \tag{46}$$

Note that if the contact material is the same for both the top and bottom of the contact, the effect mean-free-path is equal to the mean-free-path of the material, and the Sharvin resistance becomes

$$\Omega_{Sharvin} = \frac{\lambda\rho}{a} \tag{47}$$

(5.3) Constriction Resistance (Wexler Regime)

If the contact radius is comparable to the electron mean-free path of the contact material, a transition equation is used to calculate the resistance. Wexler developed the following equation

$$\Omega_{Wexler} = \Gamma(K)\left(\frac{\rho}{2a}\right) + \frac{4K\rho}{3\pi a} \tag{48}$$

where K = l/a is known as the Knudsen ratio and is used to characterize the constriction.
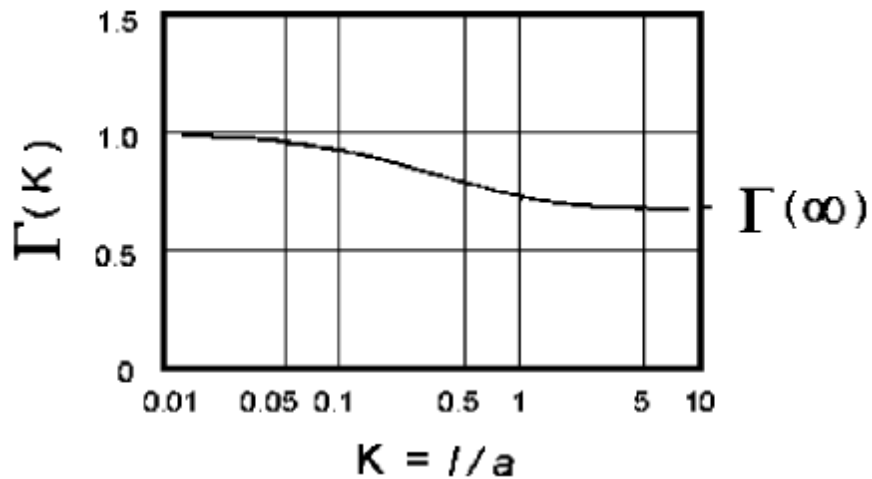
Figure 11: Plot of gamma versus K

(5.4) *Holm φ-ϑ Relation*

In his book, Holm presents a relationship between the maximum temperature in a contact and the applied electrical potential. In order to formulate this relationship, the assumption was made that the electrical current lines and the heat transfer lines are coincident.

$$\int_{T_0}^{T_0+\Theta} \rho\lambda dT = \frac{U^2}{8}$$

(49)

where T_0 is the bulk temperature far away from the contact, ρ is the electrical resistivity, λ is the thermal conductivity, and U is the applied electrical potential. Note that φ is the maximum supertemperature, or the maximum temperature measured with respect to the bulk temperature. Additionally, if the material properties can be suitably averaged over the given temperature range, Equations 49 reduces to

$$\overline{\rho\lambda}\Theta = \frac{U^2}{8}$$

(50)

6. Thermal Domain

(6.1) *General Heat Conduction Equation*

The general heat conduction equation is

$$\lambda\nabla^2 T + \nabla\lambda \cdot \nabla T + \dot{q} = \rho c \frac{\partial T}{\partial t}$$

(51)

However, assuming that we are not concerned with transient behavior, and making the assumption that the thermal conductivity is constant, this equation reduces to

$$\nabla^2 T + \frac{\dot{q}}{\lambda} = 0$$

(52)

This equation governs the heat conduction in a solid body with bulk characteristics. This behavior will be the bulk of the contact.

(6.2) *Heat Transfer Constriction*

When there is heat conduction through a constriction, such as a small contact spot, the heat conduction behaves much the same way that electric current behaves through a constriction. In fact, equivalent heat conduction equations in the form of Equations 44, 47, and 48 can be written for the thermal domain.